

ACCURATE PARAMETERS OF THE MASS DISTRIBUTION IN SPIRAL GALAXIES. I. FABRY-PEROT OBSERVATIONS OF NGC 5585

SÉBASTIEN BLAIS-OUELLETTE

Département de Physique and Observatoire du Mont Mégantic, Université de Montréal, C.P. 6128, Succursale Centre Ville, Montréal, H3C 3J7, QC, Canada; and IGRAP, Observatoire de Marseille, 2 Place Le Verrier, F-13248 Marseille Cedex 4, France; blaisous@astro.umontreal.ca

CLAUDE CARIGNAN¹

Département de Physique and Observatoire du Mont Mégantic, Université de Montréal, C.P. 6128, Succursale Centre Ville, Montréal, H3C 3J7, QC, Canada; carignan@astro.umontreal.ca

PHILIPPE AMRAM

IGRAP, Observatoire de Marseille, 2 Place Le Verrier, F-13248 Marseille Cedex 4, France; amram@observatoire.cnrs-mrs.fr

AND

STÉPHANIE CÔTÉ¹

Herzberg Institute of Astrophysics, National Research Council of Canada, 5071 West Saanich Road, Victoria, V8X 4M6, BC, Canada; stephanie.cote@hia.nrc.ca

Received 1998 December 22; accepted 1999 July 29

ABSTRACT

Using the example of the Sd galaxy NGC 5585, it is shown that high-resolution, two-dimensional H II kinematical data are necessary to determine accurately the parameters of the mass (luminous and dark) distribution in spiral galaxies. New Canada-France-Hawaii Telescope Fabry-Perot H α observations are combined with low-resolution (20") Westerbork H I data to study its mass distribution. Using the combined rotation curve and best-fit models, it can be seen that $(M/L_B)_*$ of the luminous disk goes from 0.3, using only the H I rotation curve, to 0.8, using both the optical and the radio data. This reduces the dark-to-luminous mass ratio in NGC 5585 by $\sim 30\%$ through increasing the dark matter halo core radius by nearly the same amount. This shows the importance of the inner, rising part of the rotation curve for the accurate determination of the parameters of the global mass (luminous and dark) distribution and suggests that such a fine tuning of the rotation velocities, using high-resolution, two-dimensional H II kinematics, is necessary to look at correlations between the parameters of the dark matter component and other properties of galaxies.

Key words: dark matter — galaxies: fundamental parameters —
galaxies: individual (NGC 5585, NGC 3198) — techniques: interferometric

1. INTRODUCTION

In the last 25 years, a large number of rotation curves were derived for spiral (Sp) and dwarf irregular (dIrr) galaxies from two-dimensional H I kinematics obtained with synthesis instruments such as the Westerbork synthesis radio telescope array, the Very Large Array, and the Australia Telescope (for a good review of the first 20 years, see Ashman 1992). In many galaxies, especially in late-type spiral and dIrr galaxies, the H I emission extends much farther out than that of the optical and, thus, farther out than the H II emission as well. An argument often used is that, since the H I rotation curve probes the gravitational potential in the dark matter-dominated region, it is best suited to derive the parameters of the mass distribution and especially of the dark matter halo. However, as will be shown, the parameters of the mass models (and especially of the dark matter distribution) are very sensitive not only to the flat part of the rotation curve (best probed by the H I observations) but also to the rising, inner part, which can be derived with greater precision using two-dimensional H α observations (see, e.g., Amram et al. 1992, 1994, 1995, 1996). This is also well illustrated by Swaters (1999), who clearly shows the impact of varying the position of the first few

velocity points (within the uncertainties due to “beam smearing”) on the parameters of the mass models, even in the dark matter-dominated dwarfs.

The method that is now regarded as the classical method for studying mass distribution (van Albada et al. 1985; Carignan & Freeman 1985) is illustrated in Figure 1 (*top*), which shows the analysis of the mass distribution of NGC 5585 using its H I rotation curve (Côté, Carignan, & Sancisi 1991). See also Begeman (1987), Broeils (1992), and Côté (1995) for many more examples. First, the rotation curve is obtained by fitting a “tilted ring” model to the H I velocity field in order to represent the warp of the H I disk, which is almost always present. The accuracy of the model representation is then checked by looking at the residual (data minus model) map (Warner 1973; Sancisi & Allen 1979). Then, the luminosity profile in the reddest band available to probe the mass dominant population is transformed into a mass distribution for the stellar disk, assuming a constant value of $(M/L_B)_*$ (Casertano 1983; Carignan 1985). For the contribution of the gaseous component, the H I radial profile scaled by 1.33 is used to account for He. The difference between the observed rotation curve and the computed contribution to the curve of the luminous (stars and gas) component is thus the contribution of the dark component, which can be represented by an isothermal halo (Carignan 1985) or some other functional form (see, e.g., Lake & Feinswog 1989). The model of Figure 1 (*top*) allows us to study the dark-to-luminous mass ratio as a function of radius, as

¹ Visiting Astronomer, Canada-France-Hawaii Telescope, operated by the National Research Council of Canada, the Centre National de la Recherche Scientifique of France, and the University of Hawaii.

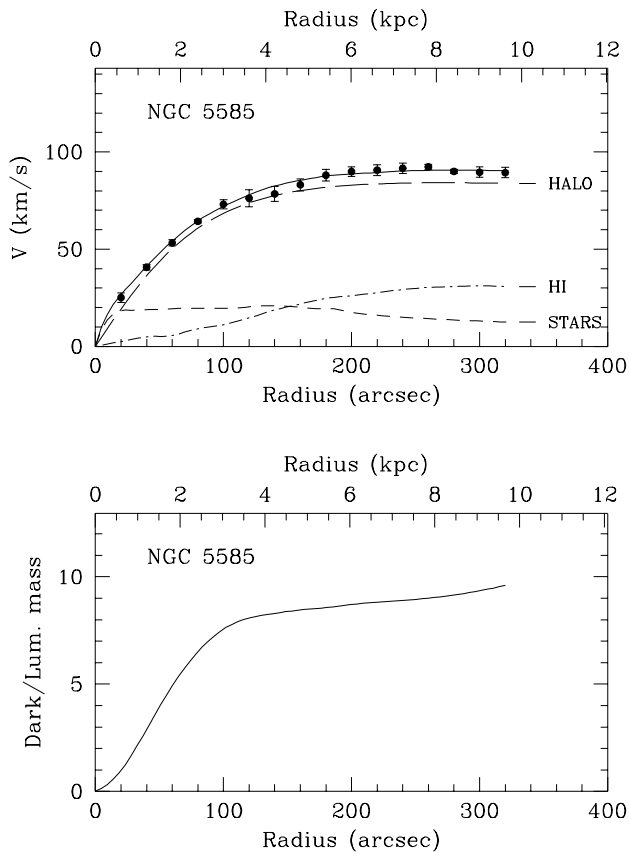


FIG. 1.—*Top*: Best-fit mass model for NGC 5585 using the H I rotation curve. The model parameters are $(M/L_B)_* = 0.3$, $r_c = 2.8$ kpc, and $\sigma = 53$ km s⁻¹. *Bottom*: Dark-to-luminous mass ratio as a function of radius.

shown in Figure 1 (*bottom*). Naturally, this is for standard gravity. Some alternative models, such as MOND, have also been explored (Milgrom 1983; Sanders 1996; McGaugh & de Blok 1998).

The example of NGC 5585 shows the importance of an accurate determination of the rising part of the rotation curve, since this is the part that mainly constrains the values of two of the three free parameters of the mass model, namely, the mass-to-light ratio of the luminous stellar disk $(M/L_B)_*$ and the core radius r_c of the dark component. The third parameter, the one-dimensional velocity dispersion σ of the dark isothermal halo is mainly constrained by the outer part of the rotation curve. The H I observations, often optimized for maximum sensitivity in the outer parts, have in most of the published studies a resolution of only 20"–45" (higher resolution is naturally possible by adding longer baselines when there is sufficient H I flux). Attempts have been made to correct for the effect of beam smearing, which can be very important in the inner parts because of the strong velocity gradient (sometimes combined with a strong radial distribution gradient) across the large H I beam. This is examined using as an example the Sc galaxy NGC 3198.

Another point that needs to be stressed is that full two-dimensional H II kinematical data are necessary for this work; one-dimensional, long-slit spectroscopy is not sufficient. This is because of the fact that the photometric parameters (we are mainly concerned with the position angle [P.A.] and photometric center in this case) used to position the slits on the galaxies can sometimes be quite different from the kinematical parameters. Naturally, if the

slit is positioned with a slightly wrong position angle, the velocities will necessarily be underestimated. This is well illustrated for the case of the rotation curves of galaxies in clusters (Whitmore, Forbes, & Rubin 1988 for one-dimensional long-slit spectroscopy; Amram et al. 1996 for two-dimensional Fabry-Perot [FP] spectroscopy).

The importance of the rising part of the rotation curve on the parameters for both the luminous and dark matter distributions is illustrated by two examples in § 2. Section 3 describes the new Canada-France-Hawaii Telescope (CFHT) FP observations and data reduction of the NGC 5585 data. The H II kinematics and optical rotation curve are discussed in § 4, while the mass models and the parameters of the mass distribution are given in § 5. Finally, § 6 gives a summary of the results and draws general conclusions from this study.

2. IMPORTANCE OF RISING PART OF ROTATION CURVE ON THE PARAMETERS OF MASS (LUMINOUS AND DARK) DISTRIBUTION

It has always been thought that the problem of beam smearing was important mainly in early-type spiral galaxies, where the strong gradient due to the presence of the bulge was attenuated in low-resolution H I data and where it was obvious that higher resolution data were necessary to see the true kinematics resulting from the centrally concentrated luminous mass distribution. In what follows, it will be shown that, while the effect of beam smearing in late-type spiral galaxies may be less dramatic, it can nevertheless have a significant impact on the derived parameters of both the luminous and dark mass distributions.

2.1. The Case of NGC 5585

To show the importance of the first few points of the rotation curve in a galaxy such as NGC 5585, a model was constructed that gives no weight to the first two points of the H I curve (Fig. 2; *top*). This model mimics a difference of less than 10" with the real position of the first two points, a very plausible effect of the large radio beams. In this model, the $(M/L_B)_*$ of the stellar disk ranges from 0.3 (Fig. 1; *top*) to 1.0 (Fig. 2; *top*), with the result that the mass of the stellar disk ranges from ~20% of the gaseous disk to a comparable mass. More importantly is that the dark matter halo is less centrally concentrated with a dark-to-luminous mass ratio ranging from 9.5 (Fig. 1; *bottom*) to 6.3 (Fig. 2; *bottom*) at the last measured point of the rotation curve. This is a difference of more than 30% in the dark-to-luminous mass ratio, for a difference of less than 10" in the position of the first two points of the curve. As illustrated in Figures 1 (*bottom*) and 2 (*bottom*), the global distribution of the dark component is also totally different. This is why we think that the ideal rotation curve to study the mass distribution in galaxies should combine the high resolution of H α FP observations in the inner parts with the high sensitivity of the low-resolution H I observations in the outer parts.

2.2. The Case of NGC 3198

Begeman (1989) published a Westerbork H I rotation curve of NGC 3198 where he attempted to correct for the effect of beam smearing. Theoretically, one should be able to calculate this effect by convolving the rapidly dropping H I density profile and the rising rotation curve inside the width of the beam. In the inner parts, his rotation velocities are systematically larger (up to 26 km s⁻¹ at 30") than the

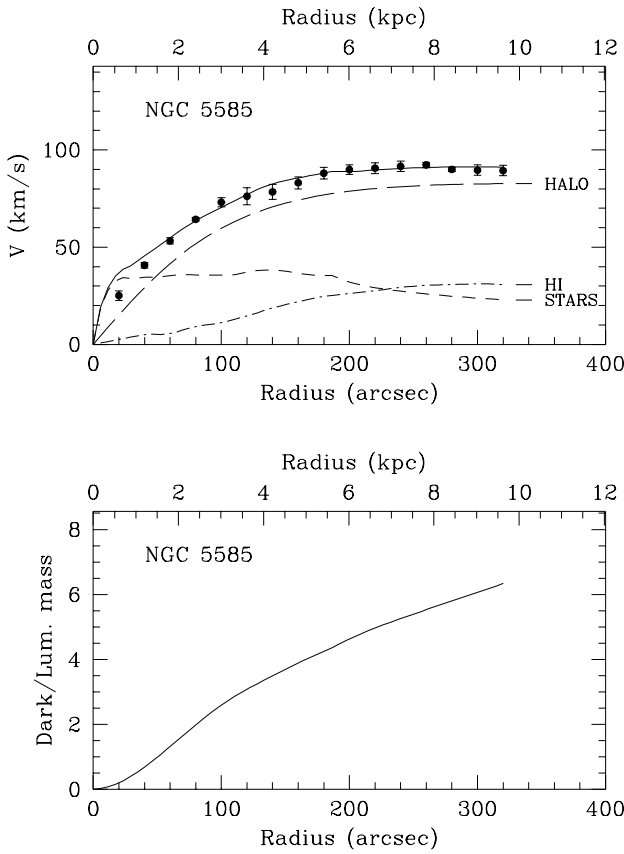


FIG. 2.—*Top*: Maximum disk mass model for NGC 5585, where the first two points of the H I rotation curve have been given zero weight. The model parameters are $(M/L_B)_* = 1.0$, $r_c = 3.5$ kpc, and $\sigma = 52$ km s⁻¹. *Bottom*: Dark-to-luminous mass ratio as a function of radius.

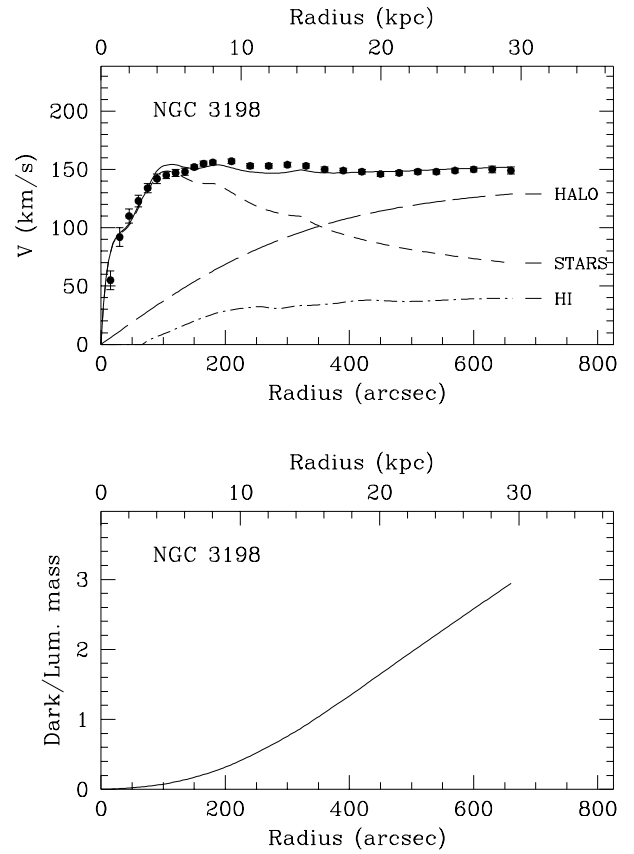


FIG. 3.—Best-fit mass model for NGC 3198 using the H I rotation curve (Begeman 1989), corrected for beam smearing. The model parameters are $(M/L_B)_* = 9.4$, $r_c = 17.2$ kpc, and $\sigma = 85.6$ km s⁻¹.

values derived in a previous H I study by Bosma (1981). If the corrections are accurate, one would expect that there should be very little gain in using high-resolution H α data. Figure 3 and Table 1 show the best-fit model using the

beam smearing-corrected H I data. It can be seen that for $r < 3$ kpc and $r > 15$ kpc, the model gives a good representation of the data. However, around 4 kpc, the model velocity is larger, by ~ 10 km s⁻¹, than the measured velocity.

TABLE 1
PARAMETERS OF THE MASS MODELS OF NGC 3198

PARAMETER	ROTATION CURVE		
	H I ^a	Combined H I ^a and H α	H I ^b
Luminous disk component:			
$(M/L_B)_* (M_\odot/L_\odot)$	9.4 ± 0.2	8.5 ± 0.3	2.8 ± 0.5
$M_* (M_\odot)$	3.2×10^{10}	2.9×10^{10}	9.6×10^9
$M_{\text{H I} + \text{He}} (M_\odot)$	6.5×10^9	6.5×10^9	6.5×10^9
Dark halo component:			
r_c (kpc).....	17.2 ± 1.0	11.7 ± 1.0	3.9 ± 0.1
σ (km s ⁻¹).....	85.6 ± 2.0	79.0 ± 1.5	83.4 ± 1.0
$\rho_0 (M_\odot \text{ pc}^{-3})$	0.004	0.008	0.076
At Holmberg radius (R_{HO}), $r \approx 13$ kpc:			
$\rho_{\text{halo}} (M_\odot \text{ pc}^{-3})$	0.002	0.002	0.002
$M_{\text{dark} + \text{lum}} (M_\odot)$	6.2×10^{10}	6.6×10^{10}	6.6×10^{10}
$(M/L_B)_{\text{dyn}}$	18	19	19.5
$M_{\text{dark}}/M_{\text{lum}}$	0.76	1.1	4.3
At last measured point, $r \approx 29$ kpc:			
$\rho_{\text{halo}} (M_\odot \text{ pc}^{-3})$	0.0005	0.0004	...
$M_{\text{dark} + \text{lum}} (M_\odot)$	1.5×10^{11}	1.4×10^{11}	...
$(M/L_B)_{\text{dyn}}$	44	41	...
$M_{\text{dark}}/M_{\text{lum}}$	2.9	3.0	...

^a Begeman 1989.

^b Bosma 1981.

A best-fit model (Fig. 4) was obtained by combining Begeman's (1989) H I data with the FP H α kinematical data of Corradi et al. (1991). We see that while the agreement between the two sets of data appears good over all, the optical velocities are somewhat smaller in the steep, rising part of the rotation curve. As can be seen in Table 1, the dark-to-luminous mass ratio at the last measured point has changed very little between the two models ($2.9 \rightarrow 3.0$), but the shape of the halo has changed substantially, becoming more centrally concentrated with r_c going from 17.2 to 11.7 kpc, again a change of more than 30%. The apparently small difference in velocity ($\sim 5 \text{ km s}^{-1}$) results in an increase of the dark halo central density ρ_0 by nearly a factor of 2 ($0.004 \rightarrow 0.008$). This suggests that Begeman (1989) may have overestimated his beam-smearing corrections.

It is instructive also to compare this result with the earlier Bosma (1981) data, which were not corrected for beam smearing, as is the case for most H I data. NGC 3198 is an Sc galaxy, in which the velocity gradient is much smaller than in Sa or Sb galaxies, and one would have thought that the effect of beam smearing should not be that dramatic. Figure 5 shows the best-fit model using that data set. We see that the mass distribution is completely different, with a much smaller disk and a dark halo that dominates completely for $r \geq 1 \text{ kpc}$. The result is that, with differences $\leq 10 \text{ km s}^{-1}$ for $0 \leq r \leq 6 \text{ kpc}$, the dark component has nearly 10 times higher central density, which results in an increase of the dark-to-luminous mass ratio from ~ 1 to ~ 4 .

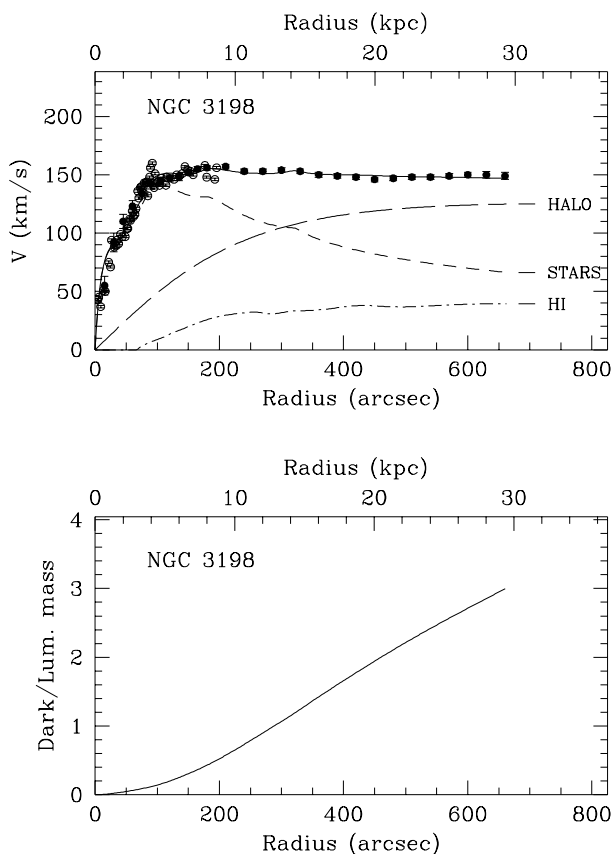


FIG. 4.—Best-fit mass model for NGC 3198 using the H I (filled circles) rotation curve (Begeman 1989) and the H α (open circles) rotation curve (Corradi et al. 1991). The model parameters are $(M/L_B)_* = 8.5$, $r_c = 11.7 \text{ kpc}$, and $\sigma = 79.0 \text{ km s}^{-1}$.

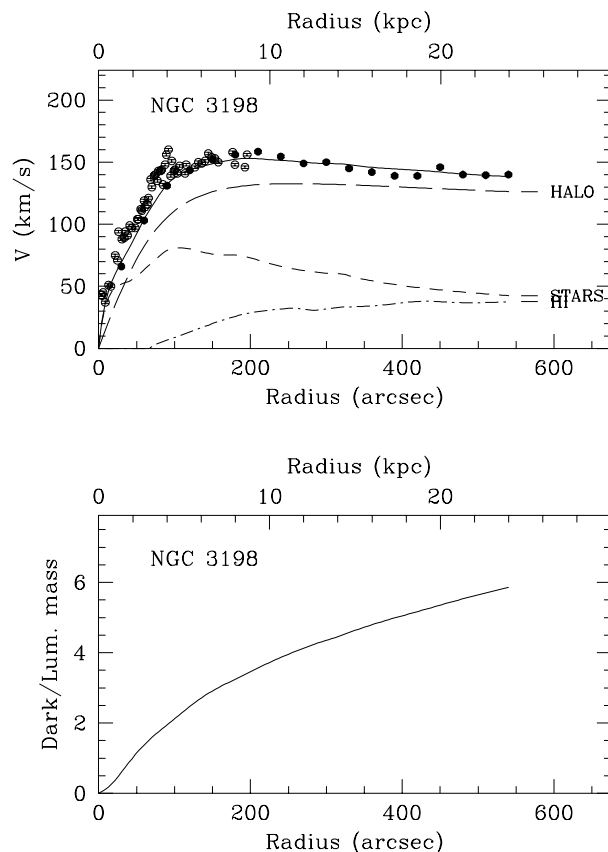


FIG. 5.—Best-fit mass model for NGC 3198 using the H I rotation curve of Bosma (1981), not corrected for beam smearing. The model parameters are $(M/L_B)_* = 2.8$, $r_c = 3.9 \text{ kpc}$, and $\sigma = 83.4 \text{ km s}^{-1}$.

Many more examples could be discussed. However, we think that the examples above show clearly that high-resolution H α data are necessary to compute accurately the parameters of both the luminous and dark mass distributions.

3. FABRY-PEROT OBSERVATIONS AND REDUCTION

Table 2 gives the optical parameters of NGC 5585, and Table 3 lists the complete observing parameters. The Fabry-Perot observations of the H α emission line were obtained in 1994 February at CFHT. The FP etalon (CFHT 1) was installed in the CFHT's multiobject spectrograph (MOS). A narrowband filter ($\Delta\lambda = 10 \text{ \AA}$), centered at $\lambda_0 = 6570 \text{ \AA}$ (nearly at the systemic velocity of NGC 5585, $V_{\text{sys}} \approx 305 \text{ km s}^{-1}$), was placed in front of the etalon. The available field with no vignetting was $\approx 8.5 \times 8.5$, with 0.34 pixel^{-1} . The free spectral range of 5.66 \AA (258 km s^{-1}) was scanned in 27 (+ 1 overlapping) channels, producing a sampling of 0.2 \AA (9.2 km s^{-1}) per channel. Eight minutes integration was spent at each channel position.

3.1. Data Analysis

Following normal debiasing and flat-fielding with standard IRAF procedures, a robust, three-dimensional, cosmic-ray removal routine, which tracks cosmic rays by spatial (pixel-to-pixel) and spectral (frame-to-frame) analyses, was applied.

Since FP systems have multiple optical surfaces, some defocalized ghost reflections can be present (Bland-Hawthorn 1995), especially since the etalon was not tilted.

TABLE 2
OPTICAL PARAMETERS OF NGC 5585

Parameter	Value
Morphological type ^a	SABd
R.A. (J2000.0)	14 ^h 19 ^m 48 ^s .1
Decl. (J2000.0)	56°43'44"
<i>l</i>	214°95
<i>b</i>	56°73
Adopted distance (Mpc) ^b	6.2 ($1' \simeq 1.8$ kpc)
Mean axis ratio, $q = b/a^c$	0.61 ± 0.01
Inclination ($q_0 = 0.12$), i°	53° ± 1°
Isophotal major diameter, D_{25}°	5'27
Major axis P.A. ^c	99° ± 1°
Exponential scale length (kpc) ^c	1.4
Holmberg radius, R_{HO}°	3.62
Absolute magnitude, M_B°	-17.5
Total luminosity, L_B	$1.5 \times 10^9 L_\odot$
Heliocentric radial velocity (km s ⁻¹) ^a	305 ± 3

^a RC3.

^b $H_0 = 75 \text{ km s}^{-1} \text{ Mpc}^{-1}$.

^c Côté et al. 1991.

To get rid of these reflections, we composed a “ghost image” by using the ghost reflection of a bright star in the field (Fig. 6) and numerically simulating a similar but scaled reflection for every pixel in the field. This image was then subtracted from the original. This procedure very efficiently removes all of the reflected continuum and adequately but not perfectly (~80%) removes the monochromatic emission.

The presence of strong night-sky lines, combined with photometric variations (transparency, seeing) from one

TABLE 3
PARAMETERS OF THE FABRY-PEROT OBSERVATIONS

Parameter	Value
Date of observations	1994 February 20
Telescope	3.6 m CFHT
Instrumentation:	
Focal plane instrument	MOS FP
CCD detector	2048 × 2048 Loral 3, $\sigma = 8 e^{-1}$
Filter	$\lambda_0 = 6570 \text{ \AA}$, $\Delta\lambda = 10 \text{ \AA}$
Fabry-Perot etalon	Scanning QW 1162 (CFHT 1)
Interference order	1155 at λ_{neon}
Mean finesse in the field	12
Calibration lamp	Neon ($\lambda = 6598.95 \text{ \AA}$)
Duration:	
Per channel	8 minutes
Total	3 hr 45 minutes
Spatial parameters:	
Field size	8.5 × 8.5
Pixel scale	0".34 pixel ⁻¹
Spectral parameters:	
Number of channels	27
Free spectral range	5.66 Å (258 km s ⁻¹)
Sampling per channel	0.2 Å (9.2 km s ⁻¹)

exposure to another, led us to proceed to a first background subtraction on each of the 27 nonredundant frames (now assembled in a three-dimensional cube). This background includes continuous, diffuse light and monochromatic emission from atmospheric OH radicals and from geocoronal H α . These backgrounds vary both spatially and temporally. Using the radial symmetry of the FP, the sky was evaluated by azimuthally summing rings of constant phase where the

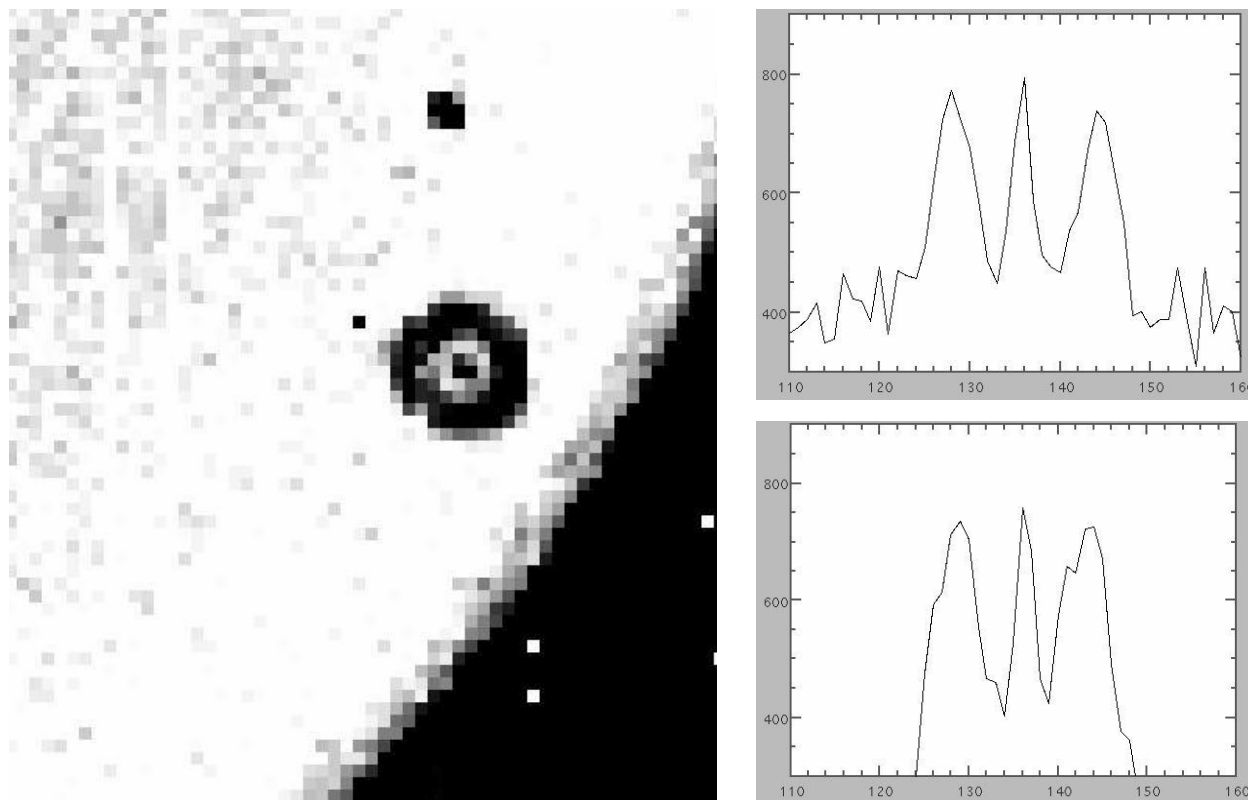


FIG. 6.—Left, real reflection of a star; top right, cut along the y-axis of the real reflection; bottom right, cut along the y-axis of the simulated reflection

galaxy signal had been masked. The computed background was then removed in each ring.

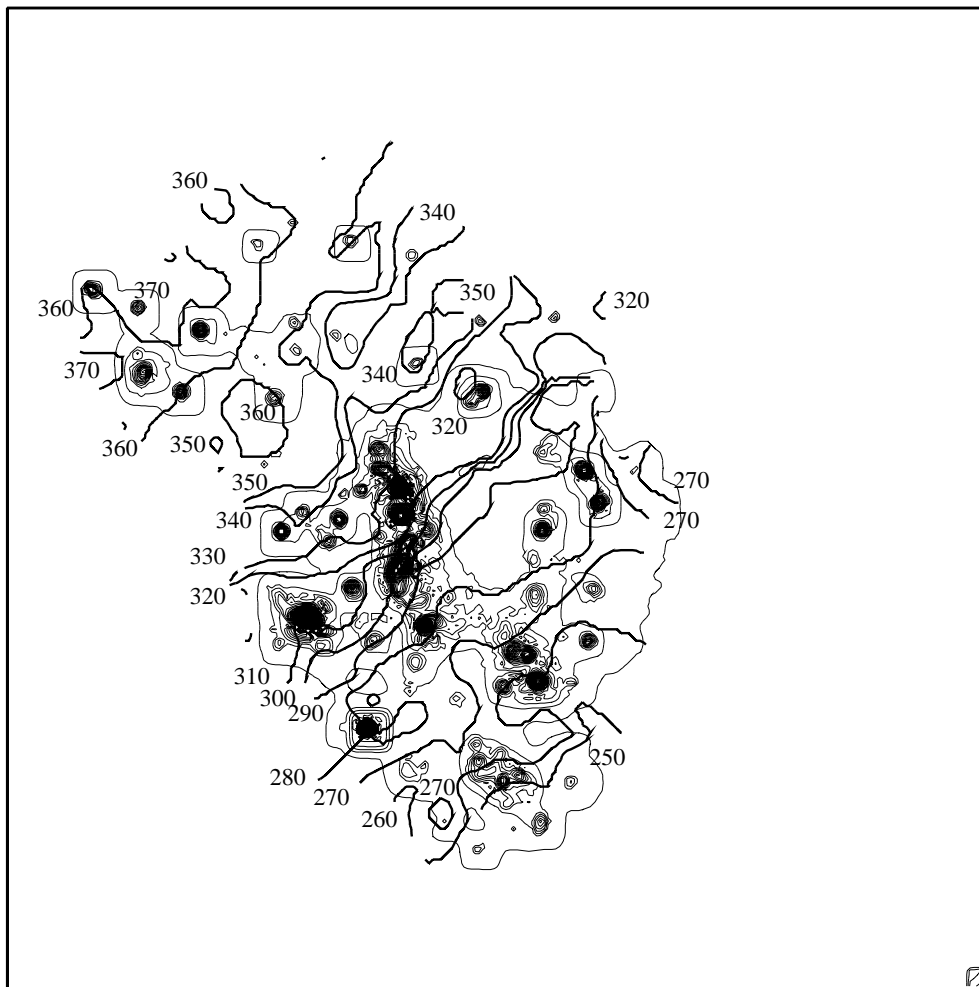
A neon calibration lamp ($\lambda 6598.95 \text{ \AA}$) was used to fix the zero point at each pixel. To be totally device independent, the theoretical position of a sky emission line was then used to fine tune the phase (wavelength origin) at each pixel in order to get a particular wavelength on an exact x - y plane. Because of limited free spectral range, this telluric line is a composite of geocoronal $H\alpha$ ($\lambda 6562.74$ or 517 km s^{-1}) and an OH line ($\lambda 6568.78$ or 532 km s^{-1}). Since there is no way to determine the relative contribution of each line, we are left with some uncertainties on the systemic velocity of the galaxy, but this does not affect the relative velocities and the rotation curve.

In order to get sufficient signal-to-noise ratio (S/N) throughout the image, two different Gaussian smoothings ($\sigma = 2.5$ and 3.5 pixels) were performed on the cube, using the ADHOC package (Boulesteix 1993). Velocity maps were then obtained using the intensity-weighted means of the $H\alpha$ peaks to determine the radial velocity for each pixel. A final, variable-resolution velocity map was constructed (Fig. 7) using higher resolution for regions with originally higher S/N.

4. H II KINEMATICS AND OPTICAL ROTATION CURVE

The rotation curve has been obtained from the velocity field following two different methods. The first estimate was made using the task ROCUR (Begeman 1987; Côté et al. 1991) in the AIPS package, where annuli in the plane of the galaxy (ellipses in the plane of sky) are fitted to the velocity field, minimizing the dispersion inside each ring. In this way, the center, systemic velocity, position angle, and inclination are evaluated. Second, the ADHOC package is used to fine tune these parameters by direct visualization and comparison with a residual velocity field. The optical rotation curve at $5''$ resolution is given in Table 4 and Figure 8. Note that there are two common ways to represent the errors on a rotation curve: the error on the mean ($\sigma/N^{1/2}$) and the velocity difference of the receding and approaching side, weighted by the number of points on each side, a method often used for the H I rotation curve. To be conservative, we took the maximum of the two values.

At intermediate radii, the approaching side of the galaxy is still affected by residual sky emission. This is caused by the lack of regions with pure sky signal in the most central rings, making the measurement of the sky emission lines less



NGC 5585

FIG. 7.—Velocity field superposed on $H\alpha$ monochromatic flux

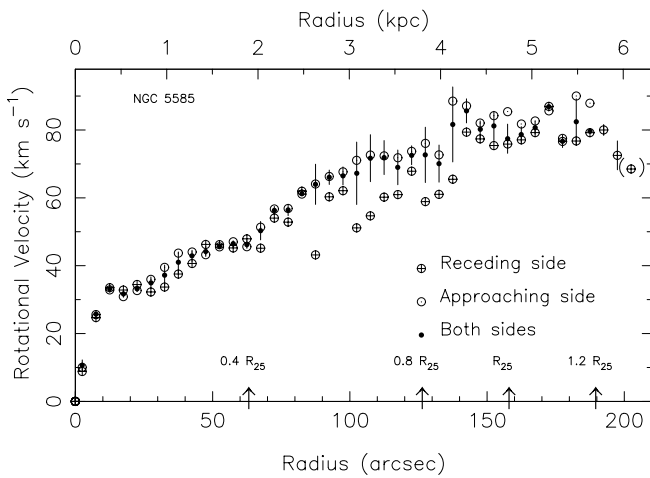


FIG. 8.—Optical rotation curve of NGC 5585

TABLE 4
OPTICAL ROTATION CURVE AT 5" RESOLUTION

Radius (arcsec)	N_{app}	V_{app} (km s ⁻¹)	N_{rec}	V_{rec} (km s ⁻¹)	V_c (km s ⁻¹)
2.5	27	10 ± 2	20	9 ± 2	11 ± 2
7.5	70	26 ± 1	59	25 ± 2	26 ± 1
12.5	104	33 ± 1	100	34 ± 1	33 ± 1
17.5	160	31 ± 1	99	33 ± 1	32 ± 1
22.5	198	33 ± 1	86	34 ± 1	33 ± 1
27.5	201	36 ± 1	100	32 ± 1	35 ± 2
32.5	195	40 ± 1	137	34 ± 1	37 ± 3
37.5	217	44 ± 1	173	38 ± 1	41 ± 3
42.5	211	44 ± 1	131	41 ± 1	43 ± 2
47.5	206	43 ± 1	125	46 ± 1	44 ± 1
52.5	194	46 ± 1	93	46 ± 1	46 ± 1
57.5	178	47 ± 1	103	45 ± 1	46 ± 1
62.5	193	46 ± 1	91	48 ± 1	46 ± 1
67.5	225	51 ± 1	54	45 ± 2	50 ± 3
72.5	270	57 ± 1	62	54 ± 2	56 ± 1
77.5	267	57 ± 1	72	53 ± 2	56 ± 2
82.5	285	61 ± 1	29	62 ± 2	61 ± 2
87.5	265	64 ± 1	6	43 ± 8	64 ± 6
92.5	288	66 ± 1	18	60 ± 4	66 ± 2
97.5	196	68 ± 1	70	62 ± 2	66 ± 3
102.5	86	71 ± 1	36	51 ± 4	67 ± 9
107.5	131	73 ± 1	17	55 ± 7	72 ± 7
112.5	105	72 ± 1	4	60 ± 2	72 ± 5
117.5	89	72 ± 1	37	61 ± 2	69 ± 5
122.5	86	74 ± 1	38	68 ± 3	73 ± 3
127.5	121	76 ± 1	48	59 ± 3	73 ± 8
132.5	179	73 ± 1	52	61 ± 1	70 ± 5
137.5	170	88 ± 1	62	65 ± 1	82 ± 1
142.5	160	87 ± 1	27	79 ± 1	86 ± 4
147.5	124	82 ± 1	56	77 ± 1	80 ± 2
152.5	72	84 ± 1	27	75 ± 2	81 ± 4
157.5	24	85 ± 1	113	76 ± 1	77 ± 4
162.5	44	82 ± 1	80	77 ± 1	79 ± 2
167.5	29	83 ± 1	35	79 ± 2	81 ± 2
172.5	1	86 ± 1	17	87 ± 2	87 ± 2
177.5	5	78 ± 5	67	77 ± 2	77 ± 2
182.5	12	90 ± 6	19	77 ± 3	82 ± 7
187.5	1	88 ± 1	20	79 ± 2	80 ± 5
192.5	0	...	30	80 ± 2	80 ± 2
197.5	0	...	13	73 ± 4	73 ± 4

NOTE.—Derived with $i = 52^\circ$, P.A. = 43° .

accurate and only partially subtracted. The final effect here is to lower the rotation velocities between 2 and 4 kpc in radius. As we will see, this is in the region where it is possible to rely with confidence on the H I data, because of the shallower fall of H I density and the slower rise of the rotation curve that make beam smearing negligible.

5. MASS MODELS AND PARAMETERS OF MASS DISTRIBUTION

The models used are described in Carignan (1985). However, instead of being “maximum disk” models, they are “best-fit” models. A χ^2 minimization technique is used in the three-parameter space of the model. Namely, those parameters are the $(M/L_B)_*$ of the stellar disk, the core radius r_c , and the one-dimensional velocity dispersion σ of the dark isothermal halo. Alternatively, one can use the central density $\rho_0 = 9\sigma^2/4\pi Gr_c^2$. The surface photometry and H I kinematics are from Côté et al. 1991.

5.1. Mass Model from the H α Rotation Curve

The best-fit mass model for the H α rotation curve at 5" resolution is shown in Figure 9. It can be seen that there is a clear sign of the disk mass in the rotation curve, which is well fitted. In fact, the best-fit model is essentially a maximum disk model. The mass-to-light ratio of the stellar disk goes from 0.3, using the H I data, to 1.0, using the H α data, which causes the halo to become less centrally concentrated. For the dark halo, the parameters are $r_c = 4.1$ kpc, $\rho_0 = 0.023 M_\odot \text{pc}^{-3}$, and $\sigma = 49.1 \text{ km s}^{-1}$, which represent

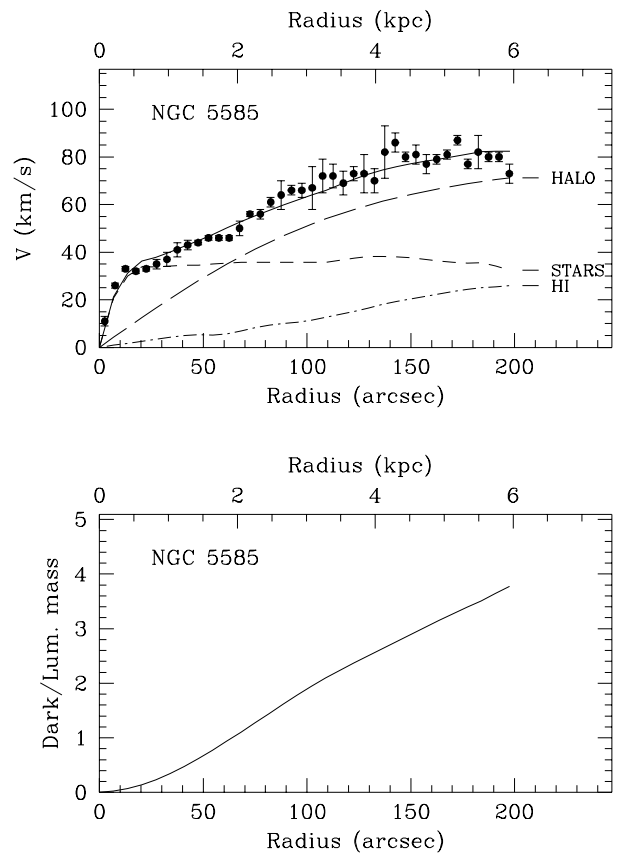


FIG. 9.—Top: Best-fit mass model for NGC 5585 using the H α rotation curve at 5" resolution. The model parameters are $(M/L_B)_* = 0.8$, $r_c = 3.7$ kpc, and $\sigma = 48 \text{ km s}^{-1}$. Bottom: Dark-to-luminous mass ratio as a function of radius.

TABLE 5
PARAMETERS OF THE MASS MODELS OF NGC 5585

PARAMETER	ROTATION CURVE		
	H I	H α	Combined H I and H α
Luminous disk component:			
$(M/L_B)_* (M_\odot/L_\odot)$	0.3 ± 0.3^a	1.0 ± 0.1	1.0 ± 0.1
$M_* (M_\odot)$	3.3×10^8	1.1×10^9	9.9×10^8
$M_{\text{H I}+\text{He}} (M_\odot)$	1.4×10^9	1.4×10^9	1.4×10^9
Dark halo component:			
r_c (kpc)	2.8 ± 0.3	4.1 ± 0.4	4.3 ± 0.4
σ (km s $^{-1}$)	52.9 ± 2.0	49.1 ± 2.0	53.6 ± 1.6
ρ_0 (M_\odot pc $^{-3}$)	0.060	0.023	0.024
At Holmberg radius R_{HO} , $r = 6.5$ kpc:			
$\rho_{\text{halo}} (M_\odot$ pc $^{-3})$	0.0035	...	0.0041
$M_{\text{dark+lum}} (M_\odot)$	1.2×10^{10}	...	1.1×10^{10}
$(M/L_B)_{\text{dyn}}$	10.6	...	10.1
$M_{\text{dark}}/M_{\text{lum}}$	8.7	...	4.6
At last measured point, $r = 9.6$ kpc:			
$\rho_{\text{halo}} (M_\odot$ pc $^{-3})$	0.0013	...	0.0017
$M_{\text{dark+lum}} (M_\odot)$	1.7×10^{10}	...	1.8×10^{10}
$(M/L_B)_{\text{dyn}}$	15.7	...	16.4
$M_{\text{dark}}/M_{\text{lum}}$	9.5	...	6.6

^a The difference between the $(M/L_B)_*$ in this paper and that in Côté et al. 1991 is a result of using a different Galactic extinction value, $A_B = 0.0$ (RC3).

a decrease of ρ_0 of more than 50%. Interestingly, the H α rotation curve provides a much better fit to the MOND model ($a_0 = 1.2 \times 10^{-8}$ cm s $^{-2}$, $M^*/L_B = 0.5$) than does the H I curve alone (see Fig. 1 of Sanders 1996). However,

the little kink seen at $r \simeq 1$ kpc could indicate the transition between the disk-dominated region and the halo-dominated region, which would exclude alternative gravitational theories based on luminous matter only. This feature could also be the dynamical signature of an inner bar, but the two-dimensional velocity field does not show evidence of non-circular motion.

It is interesting to look at the shape of the different components as a function of radius for this H α rotation curve, derived out to $\sim 1.3R_{25}$ (herein defined as $D_{25}/2$ from de Vaucouleurs et al. 1991, hereafter RC3) or $\simeq 3/3 \simeq 6.0$ kpc. In massive Sp galaxies, the stellar disk usually dominates the mass distribution for $r < R_{25}$. Typical $M_{\text{dark}}/M_{\text{lum}}$ are between 0.5 to 1.0 at that radius. This is certainly not the case here with $M_{\text{dark}}/M_{\text{lum}} \simeq 4.0$ at the last measured point of the rotation curve. Moreover, at the last point, there is almost as much luminous mass in gas as in stars. So, for a dwarf Sp galaxy such as NGC 5585, the mass distribution is much more reminiscent of what is seen in dIrr galaxies (e.g., DDO 154 [Carignan & Freeman 1988; Carignan & Beaulieu 1989] and DDO 170 [Lake, Shommer, & van Gorkom 1990]) than what is found in massive Sp galaxies (e.g., NGC 6946 [Carignan et al. 1990] and NGC 3198 [van Albada et al. 1985]). Other late-type spiral galaxies such as IC 2574 (Martimbeau, Carignan, & Roy 1994) and NGC 3109 (Jobin & Carignan 1990), both of type Sm, also have a strong contribution from dark matter, even in the inner parts, but show solid-body H I rotation curves.

5.2. Mass Model from the Combined H I and H α Rotation Curve

Table 5 presents parameter values of the mass model constructed using only the H I rotation curve, that constructed using only the H α curve, and the model from the combined H I and H α curve. For our adopted mass model of NGC 5585, we combine the high resolution of the H α data in the inner parts with the high sensitivity of the H I data in the outer parts. Since we are making a best-fit

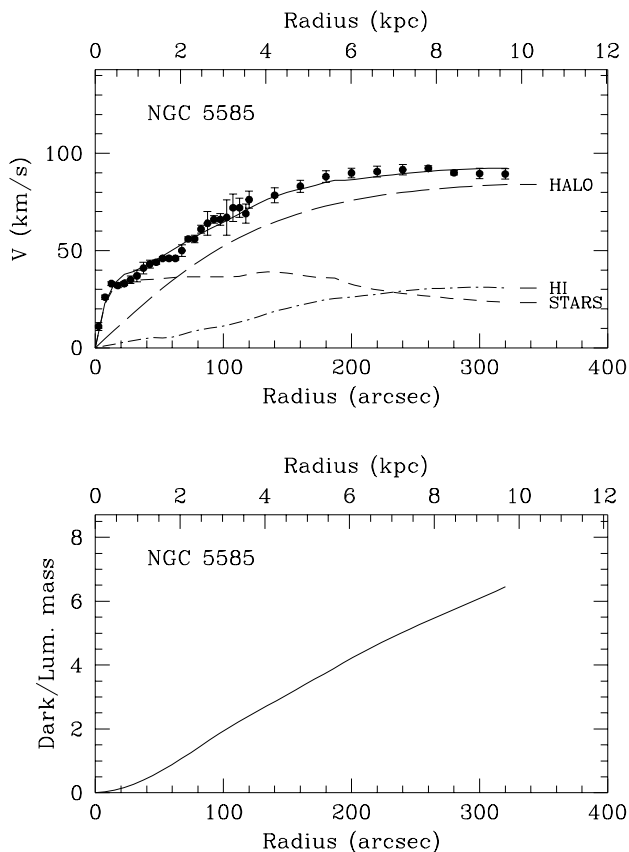


FIG. 10.—Top: Adopted best-fit mass model for NGC 5585 using the H α rotation curve for $r < 120''$ and the H I rotation curve for $r > 120''$. The model parameters are: $(M/L_B)_* = 0.8$, $r_c = 3.9$ kpc, and $\sigma = 53.3$ km s $^{-1}$. Bottom: Dark-to-luminous mass ratio as a function of radius.

model, one has to understand that, because of the higher resolution, there are more H II data points than H I data points. This means that the optical data would tend to have a greater weight than the radio data. Since optical velocities are derived from high-S/N data out to a radius of 120" and since Figure 9 of Côté et al. (1991) shows that this is the region where the H I parameters are not well defined, we decided to use for the final model the H α data for $r < 120''$ and the H I data for $r > 120''$.

This adopted model is shown in Figure 10. The parameters of the model are $(M/L_B)_* = 1.0$, $r_c = 4.5$ kpc, $\rho_0 = 0.024 M_\odot \text{pc}^{-3}$, and $\sigma = 53.6 \text{ km s}^{-1}$. As expected, σ is very similar in the combined H I and H α curve and in the H I rotation curve. This is the case because this parameter is a measure of the maximum amplitude of the rotation curve, which is mainly defined by the H I data in the outer parts. However, the two other parameters, $(M/L_B)_*$ for the stellar disk and ρ_0 of the dark halo (which are coupled), have nearly the same values as those derived with the H α curve. Again, this is because the $(M/L_B)_*$ of the luminous stellar disk, and hence the scaling parameter of the dark halo r_c , is mainly constrained by the H II data in the inner parts. Interestingly, because this newly derived central density is significantly lower, this late-type galaxy's dark halo is even less concentrated; therefore, this exacerbates the discrepancy between the observed rotation curves and those predicted by standard cold dark matter halo simulations, which are already too concentrated for late-type and dwarf galaxies (see, e.g., Navarro 1996, but see also Kravtsov et al. 1998).

6. SUMMARY AND CONCLUSIONS

The importance of an accurate determination of the rising part of a rotation curve using full two-dimensional, high-resolution Fabry-Perot observations is well illustrated by the example of NGC 5585. The principal conclusions follow.

1. The parameters of the mass distribution of both the luminous and the dark components are very sensitive to the rising part of the rotation curve (the first few velocity points), not only in early-type spiral galaxies, where the velocity gradient is large in the inner parts, but also in late-type spiral galaxies, which have a much shallower gradient. The sensitivity is especially important when the contributions of luminous and the dark matter are comparable.

2. With the example of NGC 3198, it is shown that it is very difficult to correct theoretically for the beam-smearing effect seen in radio data.

3. Full three-dimensional spectroscopy, obtained with FP spectroscopy, is to be preferred over long-slit spectroscopy in order to derive properly the orientation parameters (namely, the rotation center and the P.A.) and hence not underestimate the rotational velocities.

4. Combining new H α CFHT FP data with Westerbork H I data reduced the $M_{\text{dark}}/M_{\text{lum}}$ ratio by $\simeq 30\%$ via a decrease of the central density of nearly a factor of 3 for the late-type spiral galaxy NGC 5585. If such large errors are common, it is possible to imagine that they could mask any physical correlation between the parameters of the luminous and those of the dark matter.

5. Finally, the optimal rotation curve is clearly a combination of two-dimensional, high-resolution spectroscopy for the inner part of spiral galaxies and high-sensitivity radio observations for the outer regions.

We would like to thank the staff of CFHT for their support during the FP data acquisition and Daniel Durand from the Dominion Astrophysical Observatory, who helped with data acquisition. We also warmly thank Jacques Boulesteix for fruitful discussion on Fabry-Perot reduction and Anthony F. J. Moffat for useful comments. C. C. acknowledges grants from NSERC (Canada) and FCAR (Québec).

REFERENCES

- Amram, P., Balkowski, C., Boulesteix, J., Cayatte, V., Marcelin, M., & Sullivan, W. T. 1996, *A&A*, 310, 737
 Amram, P., Boulesteix, J., Marcelin, M., Balkowski, C., Cayatte, V., & Sullivan, W. T. 1995, *A&AS*, 113, 35
 Amram, P., Le Coarer, E., Marcelin, M., Balkowski, C., Sullivan, W. T., & Cayatte, V. 1992, *A&AS*, 94, 175
 Amram, P., Marcelin, M., Balkowski, C., Cayatte, V., Sullivan, W. T., & Le Coarer, E. 1994, *A&AS*, 103, 5
 Ashman, K. 1992, *PASP*, 104, 1109
 Begeman, K. G. 1987, Ph.D. thesis, Univ. Groningen
 ———. 1989, *A&A*, 223, 47
 Bland-Hawthorn, J. M. 1995, in *ASP Conf. Ser. 71, Tridimensional Optical Spectroscopic Methods in Astrophysics*, ed. G. Comte & M. Marcelin (San Francisco: ASP), 81
 Bosma, A. 1981, *AJ*, 86, 1791
 Boulesteix J. 1993, *ADHOC Reference Manual (Marseille: Obs. Marseille)*
 Broeils, A. 1992, Ph.D. thesis, Univ. Groningen
 Carignan, C. 1985, *ApJ*, 299, 59
 Carignan, C., & Beaulieu, S. 1989, *ApJ*, 347, 760
 Carignan, C., Charbonneau, P., Boulanger, F., & Viallefond, F. 1990, *A&A*, 234, 43
 Carignan, C., & Freeman, K. C. 1985, *ApJ*, 294, 494
 ———. 1988, *ApJ*, 332, L33
 Casertano, S. 1983, *MNRAS*, 203, 735
 Corradi, R. L. M., Boulesteix, J., Bosma, A., Capaccioli, M., Amram, P., & Marcelin, M. 1991, *A&A*, 244, 27
 Côté, S. 1995, Ph.D. thesis, Australian Natl. Univ.
 Côté, S., Carignan, C., & Sancisi, R. 1991, *AJ*, 102, 904
 de Vaucouleurs, G., de Vaucouleurs, A., Corwin, H. G., Jr., Buta, R. J., Paturel, G., & Fouqué, P. 1991, *Third Reference Catalog of Bright Galaxies (Berlin: Springer) (RC3)*
 Jobin, M. & Carignan, C. 1990, *AJ*, 100, 648
 Kravtsov, A., Klypin, A., Bullock, J. S., & Primack, J. R. 1998, *ApJ*, 502, 48
 Lake, G., & Feinswog, L. 1989, *AJ*, 98, 166
 Lake, G., Shommer, R. A., & van Gorkom, J. 1990, *AJ*, 99, 547
 Martimbeau, N., Carignan, C., & Roy, J.-R. 1994, *AJ*, 107, 543
 McGaugh, S. S., & de Blok, W. J. G. 1998, *ApJ*, 499, 66
 Milgrom, M. 1983, *ApJ*, 270, 365
 Navarro, J. F. 1996, in *ASP Conf. Ser. 117, Dark and Visible Matter in Galaxies*, ed. M. Persic & P. Salucci (San Francisco: ASP), 404
 Sancisi, R., & Allen, R. J. 1979, *A&A*, 74, 73
 Sanders, R. H. 1996, *ApJ*, 473, 117
 Swaters, R. 1999, in *ASP Conf. Ser. 182, Galaxy Dynamics*, ed. D. R. Merritt, M. Valluri, & J. A. Sellwood (San Francisco: ASP), 396
 van Albada, T. S., Bahcall, J. N., Begeman, K., & Sancisi, R. 1985, *ApJ*, 295, 305
 Warner, P. 1973, *MNRAS*, 163, 163
 Whitmore, B. C., Forbes, D. A., & Rubin, V. C. 1988, *ApJ*, 333, 542